Dynamic competition between a ligand and transcription factor NusA governs riboswitch-mediated transcription regulation

Adrien Chauvier[a,b], Pujan Ajmera[a,b], Rajeev Yadav[a,b,1], and Nils G. Walter[a,b,2]

[a]Single Molecule Analysis Group, University of Michigan, Ann Arbor, MI 48109; and [b]Center for RNA Biomedicine, Department of Chemistry, University of Michigan, Ann Arbor, MI 48109

Cotranscriptional RNA folding is widely assumed to influence the timely control of gene expression, but our understanding remains limited. In bacteria, the fluoride (F^-)-sensing riboswitch is a transcriptional control element essential to defend against toxic F^- levels. Using this model riboswitch, we find that its ligand F^- and essential bacterial transcription factor NusA compete to bind the cotranscriptionally folding RNA, opposing each other's modulation of downstream pausing and termination by RNA polymerase. Single-molecule fluorescence assays probing active transcription elongation complexes discover that NusA unexpectedly binds highly reversibly, frequently interrogating the complex for emerging, cotranscriptionally folding RNA duplexes. NusA thus fine-tunes the transcription rate in dependence of the ligand-responsive higher-order structure of the riboswitch. At the high NusA concentrations found intracellularly, this dynamic modulation is expected to lead to adaptive bacterial transcription regulation with fast response times.

cotranscriptional folding | RNA polymerase pausing | NusA | riboswitch | single-molecule fluorescence microscopy

In order to thrive, bacteria must constantly adjust their gene expression to their ever-changing environment. Because of the competition between species, it is crucial for their survival that bacteria adapt quickly to transient nutritional resources as well as external threats such as antibiotics and toxins (1). Modulation of gene expression can be achieved in multiple ways. One mechanism bacteria employ is based on riboswitches, structural noncoding RNA elements mostly found in the 5′ untranslated regions (5′-UTR) of messenger RNA (mRNA) (2). Bacterial riboswitches regulate gene expression either at the level of transcription elongation or translation initiation (3). A typical riboswitch contains two interconnected domains: 1) a conserved aptamer region able to recognize a specific ligand whose binding induces conformational changes in the second domain and 2) the expression platform that modulates the expression level of the downstream gene(s). In the case of a transcription regulation mechanism, ligand binding to the riboswitch either promotes or prevents the formation of an intrinsic terminator hairpin that leads to the premature termination of transcription (4). It has also been shown that structural alterations of the nascent RNA as a function of ligand binding can drive the recruitment of Rho termination factor to the nascent mRNA to promote transcription termination (5–7).

The archetypical fluoride (F^-)-sensing riboswitch (also termed the *crcB* motif) from the gram-positive bacterium *Bacillus cereus* controls the expression of the F^- toxicity resistance gene *crcB* through a transcriptional mechanism in which ligand binding to the aptamer prevents the formation of an intrinsic terminator hairpin in the expression platform to promote transcription readthrough (8) (Fig. 1*A*). Recent mechanistic studies of this and other riboswitches have demonstrated that the transcriptional machinery can significantly contribute to accurate

riboswitch folding and regulation (5, 9, 10). This interplay highlights the need to perform analyses with an elongation complex (EC) (i.e., with both the DNA template and transcribing RNA polymerase [RNAP]) present) to more closely mimic the natural biological context.

In addition to the structural and environmental framework provided by the EC, the transcription rate imposes kinetic constraints on riboswitch activity by affecting the time window available for efficient ligand sensing (11) or by modulating the adoption of transient functional RNA structures (5, 12). Accordingly, intrinsic RNAP pausing as an off-pathway kinetic step that interrupts the nucleotide addition cycle of the enzyme can exert an additional layer of transcriptional control (5, 7, 10, 13). RNAP pause sites play important roles in modulating gene expression, including transcription–translation coupling (14, 15), RNA folding (16), transcription termination (17), and transcription factor recruitment (18). RNAP pausing relies on specific DNA sequences embedded throughout the genome (19) but can also be promoted by the formation of RNA structures in the vicinity of the RNA exit channel (10) or the interaction with specific transcription factors (20).

Significance

Transcriptional pausing by RNA polymerases (RNAPs) is critical for genetic regulation, yet how RNA structures modulate this universal process is poorly understood. Combining biochemical and single-molecule fluorescence approaches, we here uncover a dynamic interplay between nascent messenger RNA structure and transcription factor NusA in modulating transcriptional pausing. Transcription factor NusA binds highly reversibly to the elongation complex to fine-tune the transcription rate. We find that ligand-induced riboswitch folding within the RNAP exit channel promotes transcriptional pausing, whereas it prevents NusA recruitment to the paused elongation complex. Taken together, our data reveal a dynamic model of transcription factor trafficking mediated by RNA cotranscriptional folding, expanding our understanding of the general transcription process.

www.manaraa.com

Fig. 1. Transcriptional regulation induced by the F⁻ riboswitch. (*A*) The F⁻ riboswitch from *B. cereus* regulates gene expression at the transcriptional level. Stabilization of the pseudoknot (PK) upon F⁻ binding (F⁻) prevents the formation of an intrinsic terminator hairpin, leading to the transcription of the downstream gene. Magnesium ions that coordinate ligand binding to the aptamer are indicated as orange spheres based on the previous crystal structure of a related riboswitch (47). (*B*) F⁻-dependent single-round transcription assay of a DNA template containing the 5′-UTR of the *crcB* gene from *B. cereus*. Transcription reactions were performed using the *E. coli* RNAP with 100 μM rNTPs, in the absence (*Top*) and presence (*Bottom*) of 100 nM NusA factor. The ^{32}P-labeled products were resolved on 6% polyacrylamide denaturing gel separating the full-length (FL) and terminated (T) RNA products. (*C*) Plot of the fraction of transcription readthrough versus the concentration of F⁻ ion in the absence (black) and presence (orange) of 100 nM NusA factor. T_{50} are highlighted as vertical dotted lines and are reported in *SI Appendix*, Table S2. Error bars represent the SD of the mean from independent replicates.

N-utilizing substance A protein (NusA) is an essential transcription factor that modulates transcription speed using a multitude of protein and RNA binding interactions. It is a component of the phage λ protein *N*-mediated antitermination system (21) and is required, along with other transcription factors, for the processive transcription of ribosomal RNA (22, 23). NusA promotes transcription termination (24, 25), decreases the overall speed of RNAP (26), stimulates hairpin-stabilized pauses (27–29), and participates in the correct folding of the RNA component of ribonuclease (RNase) P (30). Sigma (σ) factors occupy the same binding site on RNAP as NusA (31, 32), and the latter was found to be always bound to the EC during the elongation phase of transcription (33). NusA is a multidomain protein whose N-terminal domain is necessary and sufficient for stimulating RNAP pausing by directly contacting the RNAP exit channel (27, 28). This domain is followed by three RNA binding domains (27, 28, 34) and, finally, in *Escherichia coli*, the NusA carboxyl-terminal domain with two acidic repeats, AR1 and AR2, that directly interact with the α subunit of RNAP (32). The latter contact induces release of the autoinhibitory AR2-KH1 interaction, which then allows the S1, KH1 and KH2 domain to also interact with the nascent RNA transcript (35). Despite this detailed structural understanding and the proximity of NusA and the nascent RNA transcript at the RNAP exit tunnel, to date, there are only few examples of NusA modulating riboswitch-based transcription regulation. Specifically, it was demonstrated that the time window for ligand sensing is widened in the presence of NusA, therefore allowing for a more efficient gene regulatory response (11, 36,

37). However, a full mechanistic understanding of how NusA interacts with cotranscriptionally folding RNA has remained elusive.

In the present work, we use the F⁻ riboswitch as a model system to study the interplay between transcription factor NusA and a highly structured, regulatory RNA transcript. By employing a combination of biochemical and single-molecule approaches to a reconstituted EC, we discover an interactive mechanism wherein the cotranscriptional formation of a specific RNA structure accelerates the continuous release of NusA from the EC and thereby modulates the transcription rate. Our results also uncover how a noncoding RNA integrates multiple physiological signals for a fast gene expression response, paving the way for the design of antibiotics targeting such highly dynamic and adaptive bacterial transcription regulation systems. Indeed, since NusA is essential for bacterial viability (38, 39), further characterization of the mechanisms that modulate its association and stability to the transcription complex is a significant contribution for the design of antibiotic drugs targeting this versatile transcription factor (40).

Results

NusA Promotes Transcription Termination by Decreasing the Rate of Transcription. To test whether NusA affects the gene regulatory response of the F⁻ riboswitch, we performed single-round in vitro transcription assays of the riboswitch using bacterial (*E. coli*) RNAP with a range of F⁻ ligand concentrations (Fig. 1*B*). In the absence of NusA, we obtained a T_{50} (i.e., the concentration of F⁻ needed to induce 50% transcription readthrough) of 410 ± 40 μM (Fig. 1*C* and *SI Appendix*, Table S2), within error of the same value as the one previously reported (41). Strikingly, adding *E. coli* NusA during transcription led to a significant, twofold increase (*P* value < 0.05) in T_{50} value (840 ± 120 μM), suggesting that NusA impairs ligand binding and promotes transcription termination. Similar results were obtained while transcribing the riboswitch with the RNAP and NusA factor from *Bacillus subtilis* (*SI Appendix*, Fig. S1*A* and Table S2), showing that riboswitch folding and NusA-mediated regulation of transcription are conserved across the gram-negative (*E. coli*) and gram-positive (*B. subtilis*) transcription machineries (42).

When we increased the transcription assay concentration from 100 μM of each ribonucleoside tri-phosphate (rNTP) to a more physiological concentration of 1 mM of each rNTP in the absence of both NusA and the ligand, the percentage of readthrough product significantly increased (from 24% at 100 μM to 45% at 1 mM rNTPs) and less of an F⁻-mediated antitermination increase could be detected (decreased to a maximum of 80% at 100 μM versus only 55% at 1 mM of each rNTP; Fig. 1*C* and *SI Appendix*, Fig. S1*B*). Nevertheless, in the presence of NusA, a similar twofold increase in T_{50} value was observed (from 957 μM in the absence of to 1,723 μM in the presence of transcription factor; *SI Appendix*, Table S2), suggesting that the loss of ligand sensitivity upon addition of NusA also occurs under near-cellular transcription rate conditions.

The observation that the termination amplitude depends on the rNTP concentration raises the prospect that RNAP speed matters. Indeed, an even slower transcription at only 10 μM of each rNTP leads to more efficient transcription termination in the absence of NusA, increasing from 45% at 1 mM rNTPs to 80% at 10 μM rNTPs in the absence of F⁻ (*SI Appendix*, Fig. S1*C*). The T_{50} value significantly increased in this condition (to 1,740 ± 390 μM; *SI Appendix*, Table S2), which suggests that the ligand-free state of the riboswitch is favored at the slowest transcription rate. Most significantly, no further significant effect of NusA on the T_{50} value was observed, indicating that the thermodynamic equilibrium for ligand binding has reached
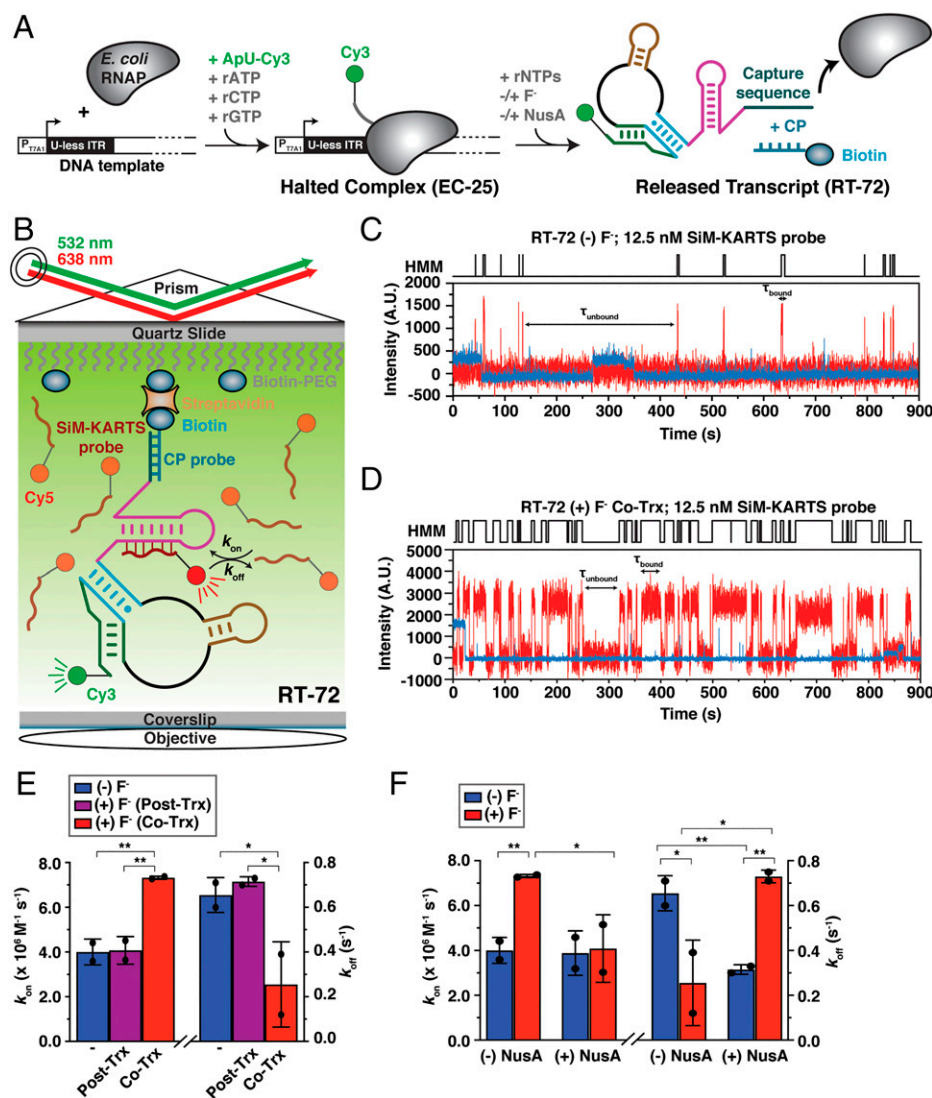
Fig. 2. Probing the structural dynamic of cotranscriptionally folded RNA. (*A*) Nascent fluorescently labeled RNA transcripts are transcribed in vitro using *E. coli* RNAP. The halted complex (EC-25) is prepared through the addition of a dinucleotide labeled with Cy3 (ApU-Cy3) and UTP deprivation (ATP/CTP/GTP) to halt the RNAP at the end of the U-less ITR. Once the transcription is completed, the released transcript (RT-72) is hybridized with a 5′-biotinylated CP for subsequent immobilization on the microscope slide. (*B*) SiM-KARTS experimental setup. Immobilization of the nascent RNA transcript on the microscope slide occurs through the CP. Repeated bindings of the SiM-KARTS probe targeting the terminator hairpin of the nascent transcript are monitored through direct excitation of the Cy5 fluorescent dye. (*C*, *D*) Representative single-molecule trajectories showing the SiM-KARTS probe binding (red) to the terminator hairpin of the F⁻ riboswitch transcribed with 1 mM rNTPs and recorded in the absence (*C*) or presence (*D*) of 2.5 mM F⁻ ion added cotranscriptionally (F⁻ Co-Trx). Hidden Markov modeling (HMM) is indicated on the top of each trace. A.U., arbitrary unit. (*E*) Histograms displaying the overall binding (k_{on}) and dissociation (k_{off}) rate constants of the SiM-KARTS probe binding to the cotranscriptionally folded F⁻ riboswitch in the absence (blue) and presence of 2.5 mM F⁻ ion added either post- (purple) or cotranscriptionally (red). Error bars are the SD of the mean from independent replicates. The total number of molecules analyzed is as follows: (−) F⁻ = 189; (+) F⁻ Post-Trx = 157; (+) F⁻ Co-Trx = 69 (***P < 0.01, **P < 0.05, *P < 0.1). (*F*) Histogram displaying the overall binding (k_{on}) and dissociation (k_{off}) rate constants of the SiM-KARTS probe binding to the cotranscriptionally folded F⁻ riboswitch in the absence and presence of 100 nM NusA factor and F⁻ ion during the transcription process. Error bars are the SD of the means from independent replicates. The total number of molecules analyzed is as follows: (−) NusA, (−) F⁻ = 189; (−) NusA, (+) F⁻ Co-Trx = 69; (+) NusA, (−) F⁻ = 110; (+) NusA, (+) F⁻ Co-Trx = 118 (***P < 0.01, **P < 0.05, *P < 0.1).

its lower limit and is no longer affected by any further NusA modulation of RNAP speed (43, 44).

Together, our results are consistent with the notion that NusA modulates the riboswitch-mediated regulation of gene expression by decreasing the overall rate of transcription, which promotes the formation of the terminator hairpin, itself antagonized by F⁻ ligand binding.

The Transcription Rate Modulates Termination Efficiency through Stabilization of the Terminator Hairpin. To better characterize the cotranscriptional folding of the riboswitch terminator hairpin as

a function of ligand concentration, we designed an in vitro transcription assay that generates a cotranscriptionally folded RNA with a single fluorophore on the 5′-end for detection at the single-molecule level (Fig. 2*A*). To this end, transcription was performed with *E. coli* RNAP and initiated with a 5′ Cy3-labeled dinucleotide (ApU-Cy3) in the presence of only three rNTPs added (with rUTP omitted), generating a labeled, active EC halted at position 25 (EC-25), where the first rUTP incorporation is needed after transcription of a U-less internal transcript region (ITR) sequence inserted upstream of the riboswitch (*Methods*). Upon addition of all four rNTPs, the

Chauvier et al.
Dynamic competition between a ligand and transcription factor NusA governs riboswitch-mediated transcription regulation

PNAS | 3 of 12
https://doi.org/10.1073/pnas.2109026118

www.manaraa.com

synchronized halted ECs are released, and transcription elongation continues past position 25, with the RNA transcript folding cotranscriptionally prior to the single-molecule probing assay (*SI Appendix*, Fig. S2*A*). To suppress heterogeneity of the transcript, as would be caused by intrinsic transcription termination at the poly-uracile sequence, the transcribed riboswitch sequence is ended to form a "released transcript" at the RNAP pause position 72 prior to the termination region (RT-72) (Fig. 2*A* and *SI Appendix*, Fig. S1*A*). Once released from transcription, RT-72 hybridizes to a subsequently added excess of biotinylated DNA capture probe (CP) with complementarity to a capture sequence inserted at the 3′-end. A radioactive in vitro transcription assay performed with fluorescently labeled dinucleotide shows that the addition of Cy3 at the 5′-end of the RNA has no effect on the ability of the riboswitch to direct transcription readthrough upon ligand addition (*SI Appendix*, Fig. S2*B* and Table S2).

The resulting nascent RT-72:CP complex was then immobilized on polyethylene glycol (PEG)-passivated and streptavidin-coated quartz slides for imaging via prism-based total internal reflection fluorescence (TIRF) microscopy. We added a short (eight-nucleotide) Cy5-labeled DNA oligonucleotide as a single-molecule kinetic analysis of RNA transient structure (SiM-KARTS) probe against the 5′ segment of the terminator stem (targeting G42-A49), which allows for probing the accessibility of this particular switching region (45, 46) (Fig. 2*B* and *SI Appendix*, Fig. S1*A*). Upon simultaneous excitation of Cy3 and Cy5, single molecules were located on the microscope slide through their Cy3 (green) RT-72 fluorescence, whereas SiM-KARTS probe binding events to the target RNA were detected as spikes of fluorescence intensity in the Cy5 (red) channel (Fig. 2 *C* and *D*).

The cumulative dwell time distributions of the SiM-KARTS probe being bound (τ_{bound}) or unbound ($\tau_{unbound}$) to the riboswitch terminator stem were fitted with double-exponential functions to extract the corresponding dissociation (k_{off}) and binding (k_{on}) rate constants, respectively (Fig. 2*E* and *SI Appendix*, Table S3). In the absence of F⁻, the SiM-KARTS probe binds to the RNA target with two rate constants of 4.69 ± 0.01 × 10⁶ M⁻¹ · s⁻¹ ($k_{on,1}$ − fraction 57%) and 0.52 ± 0.01 × 10⁶ M⁻¹ · s⁻¹ ($k_{on,2}$ − fraction 43%) and dissociates with two rate constants of 0.41 ± 0.01 s⁻¹ ($k_{off,1}$ − fraction 94%) and 0.02 ± 0.01 s⁻¹ ($k_{off,2}$ − fraction 6%). This finding is consistent with the notion that the SiM-KARTS probe senses (at least) two alternative structures of the riboswitch expression platform. Indeed, the targeted G42-A49 region is known to either form the terminator hairpin or adopt a less stable pseudoknot-like structure in the presence of ligand (9). In addition, a control experiment probing the terminator hairpin in the absence of the aptamer domain indicates that the pseudoknot structure contributes to the stability of the SiM-KARTS to the RNA target, increasing the dissociation rate constant in the context of RT-72 (*SI Appendix*, Fig. S2 *C–E* and Table S3).

We transcribed the RT-72 riboswitch in the absence of ligand and then immobilized the RNA and added a saturating concentration of F⁻ (2.5 mM, based on the titration in Fig. 1*C*), which led to no significant change in the kinetic parameters observed (F⁻ Post-Trx, Fig. 2*E*). This is consistent with the expectation that ligand-mediated modulation of the terminator hairpin structure cannot occur after the transcription process, in agreement with a kinetically regulated riboswitch (37). In further support of this, when we instead added ligand already during the transcription process, a significant change in the kinetic parameters of the SiM-KARTS probe with more frequent and longer binding events was observed (F⁻ Co-Trx, Fig. 2 *D* and *E*). In addition to an increase of the k_{on} values, a significant change also occurs in the amplitude of the fast association rate, which now contributes >90% of the overall k_{on}. This observation supports that ligand

binding to the riboswitch promotes the adoption of a less-structured terminator hairpin (9). Furthermore, the overall τ_{bound} of the SiM-KARTS probe is significantly increased in the presence of F⁻. In fact, short (0.36 ± 0.01 s⁻¹) and long (0.05 ± 0.01 s⁻¹) binding events are almost equally distributed in the ligand-bound state (*SI Appendix*, Table S3). Lastly, the decrease in the overall dissociation rate constant indicates that ligand binding leads to a partial destabilization of the terminator hairpin. Our SiM-KARTS analysis of cotranscriptionally folded RNA transcripts thus supports that F⁻ binding to the riboswitch shifts the dynamic sampling toward antitermination through terminator hairpin destabilization.
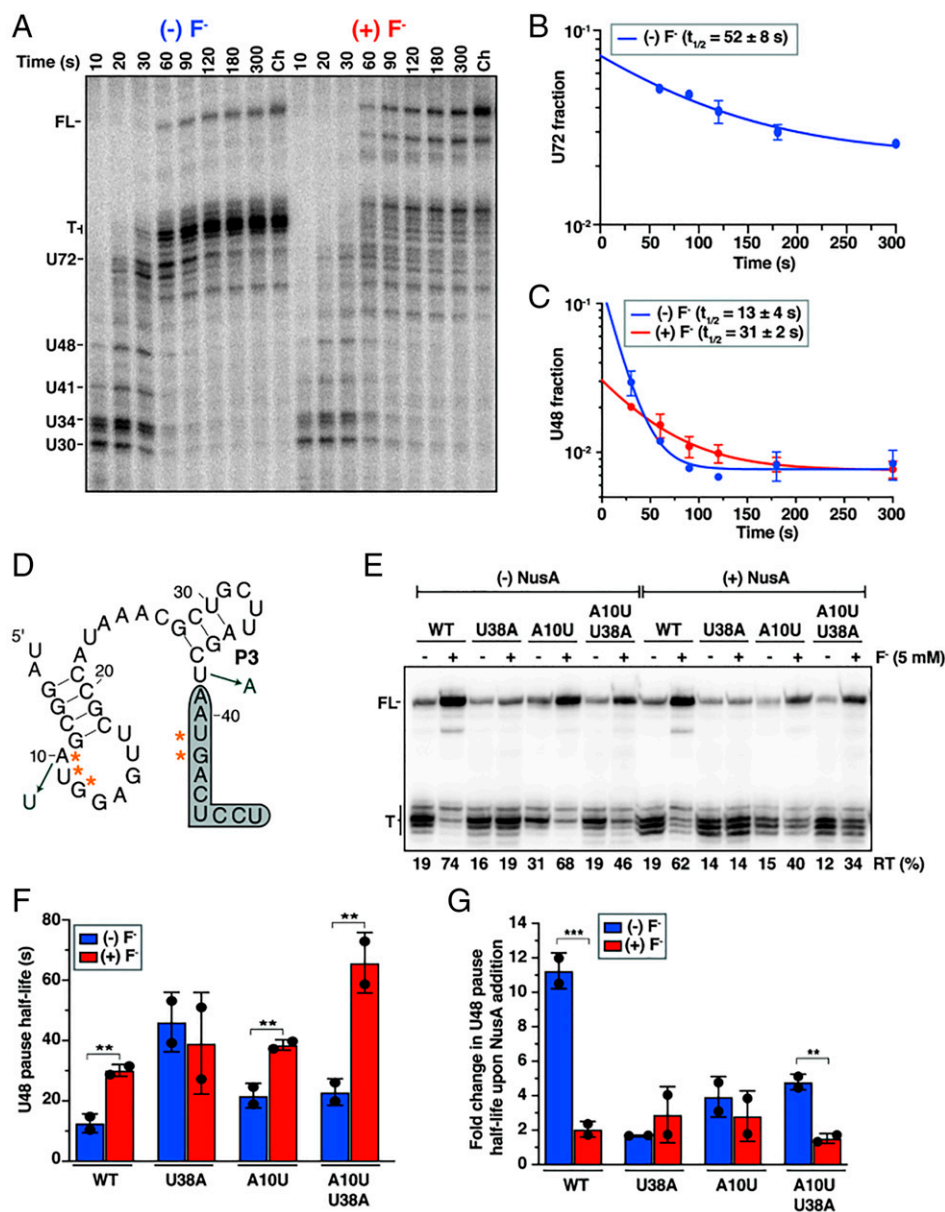
The addition of NusA during the transcription has no significant impact on the association rate constants of the SiM-KARTS probe in the absence of F⁻, but a significant decrease in the dissociation rate constant is observed (Fig. 2*F* and *SI Appendix*, Table S3), showing that NusA shifts the equilibrium toward the folding of the terminator hairpin similarly to the same structure in the absence of the competing pseudoknot (*SI Appendix*, Fig. S2). However, the overall k_{on} of the SiM-KARTS probe significantly decreased when NusA and F⁻ were both present during transcription (Fig. 2*F*). This observation indicates that NusA impedes the ligand-mediated switching mechanism by promoting cotranscriptional folding of the terminator hairpin specifically in the ligand-bound state. Moreover, the presence of F⁻ does not shift the distribution of the fast and slow dissociation rate constants, which suggests that NusA also prevents the destabilization of the terminator hairpin induced by pseudoknot formation in the ligand-bound state. Moreover, similar results were obtained at a lower transcription rate (*SI Appendix*, Fig. S3 and Table S3).

Taken together, we conclude that NusA antagonizes the ligand-induced structural change of the riboswitch mediating antitermination by lowering the overall transcription rate, which ultimately promotes formation and stabilization of the terminator hairpin.

Ligand-Induced Structural Change Modulates RNAP Pausing Efficiency. Our biochemical and single-molecule assays underscore the importance of the transcription rate for riboswitch folding and downstream regulation of transcription termination. Transcriptional pausing has been shown to be an inherent parameter that can be modulated by cotranscriptional RNA folding or protein recruitment and vice versa (20). Therefore, we next evaluated how riboswitch folding modulates transcriptional pausing, using single-round transcription assays (Fig. 3*A*).

While the RNAP pauses identified in the riboswitch aptamer domain (U30, U34, and U41) showed no significant impact of F⁻ on upstream pause duration (*SI Appendix*, Fig. S5*B* and Table S4), two pause sites found in the expression platform region (U48 and U72) are sensitive to the presence of ligand (Fig. 3 *B* and *C*). The downstream-most pause (U72) is located in the vicinity of the termination region and is not detected in the presence of ligand. Therefore, we hypothesized that cotranscriptional folding of the terminator hairpin in the ligand-free state promotes RNAP pausing and constitutes the pause signal at U72. Indeed, a SiM-KARTS assay interrogating the terminator hairpin in the context of a paused elongation complex (PEC) located at pause site 72 (PEC-72) supports the idea that the switching between terminator and antiterminator stem occurs at this pause site and participates in the regulation of transcriptional pausing at this position (*SI Appendix*, Fig. S4 and Table S3).

Interestingly, the duration of the upstream U48 pause is significantly enhanced in the presence of F⁻ (Fig. 3*C*), suggesting that the ligand-bound state further promotes RNAP pausing at this position. Upon examination of the riboswitch secondary structure, we hypothesized that the formation of the long-range

www.manaraa.com

Fig. 3. Effect of F⁻ binding on transcriptional pausing and NusA activity. (*A*) Representative denaturing gel showing the RNAP pauses during the transcription of the F⁻ riboswitch. The positions of the different pause species are indicated on the left along with the termination (T) and the full-length (FL) products. Experiments were performed using 10 μM rNTPs in the absence of 5 mM F⁻ ion. The chase lanes (Ch) were taken at the end of the time course after an additional incubation with 500 μM rNTPs for 5 min. (*B*) Fraction of complexes at the U72 pause as a function of the transcription time in the absence of F⁻ ion. Pausing at U72 was not detectable in the presence of F⁻. The reported errors are the SD of the mean independent replicates. (*C*) Fraction of complexes at the U48 pause as a function of the transcription time in the absence (blue) and presence (red) of 5 mM F⁻ ion. The reported errors are the SD of the mean from independent replicates. (*D*) Sequence and secondary structure of the F⁻ riboswitch in the context of the PEC at the U48 position. RNA nucleotides sequestered in the RNA–DNA hybrid are shadowed in gray. Mutations of the long-range interaction (A10U and U38A) used in this study are indicated in Mediterranean blue. Nucleotides that are coordinated with magnesium ions for fluoride binding are marked with orange stars. (*E*) Representative denaturing gel showing termination and antitermination in the absence (−) and presence (+) of fluoride ion (F⁻) in the context of the WT and mutants of the A10–U38 long-range interaction. Transcriptions were performed in the absence or presence of 100 nM NusA factor. Percentages of readthrough are indicated at the bottom of the gel. (*F*) Quantification of the U48 pause half-life in the WT, U38A, A10U, and A10U/U38A riboswitch variants in the absence of NusA factor. Experiments were performed using 10 μM rNTPs in the absence (blue) and presence (red) of 5 mM F⁻ ion. Error bars are the SD of the mean from independent replicates (***$P < 0.01$, **$P < 0.05$, *$P < 0.1$). (*G*) Fold-change enhancement of U48 pause half-life in the WT, U38A, A10U, and A10U/U38A riboswitch variants in the presence of 100 nM NusA factor relative to the same condition in the absence of the transcription factor. Experiments were performed using 10 μM rNTPs in the absence (blue) and presence (red) of 5 mM F⁻ ion. Error bars are the SD of the mean from independent replicates (***$P < 0.01$, **$P < 0.05$, *$P < 0.1$).

interaction A10–U38 in the ligand-bound state (47) inside the enzyme's RNA exit channel (Fig. 3*D*) could potentially stabilize RNAP pausing. To assess the impact of this long-range interaction on RNAP pausing, we mutated A10 to U10 and U38 to A38 individually and then together (Fig. 3 *E* and *F* and *SI Appendix*, Table S4). With the U38A mutant, the impact of F⁻ on RNAP pausing efficiency is completely abolished. Importantly, a mutation predicted to prevent the second A40–U48 long-range interaction (A40C construct) (47) significantly affects neither ligand sensing nor NusA-mediated regulation of transcription termination (*SI Appendix*, Fig. S5*C* and Table S2). These results demonstrate how critical the A10–U38 interaction is for ligand-mediated regulation of transcriptional pausing. In further support, the compensatory mutant (A10U/U38A) showed the same ligand-mediated effect on the U48 pause as the wild-type (WT) RNA, suggesting that positioning

the long-range A10–U38 interaction within the RNA exit channel further enhances RNAP pausing in the presence of F⁻.

To evaluate the relationship between riboswitch folding and NusA activity, we next analyzed the RNAP pausing efficiency in the presence of NusA. Overall, each pause encountered during the riboswitch transcription is, to some extent, sensitive to NusA in the absence or presence of ligand (*SI Appendix*, Fig. S5*B* and Table S4). Interestingly, in the absence of F⁻ we observed an ∼10-fold increase of the U48 pause half-life in the WT upon addition of NusA (13 s in the absence of versus 140 s in the presence of NusA) (Fig. 3 *F* and *G* and *SI Appendix*, Table S5). In contrast, in the presence of F⁻, NusA increased the U48 pause half-life only by twofold (31 s in the absence of versus 61 s in the presence of NusA). This suggests that the F⁻-bound conformation of the riboswitch may prevent NusA-mediated enhancement of U48 pausing efficiency.

Because we identified the A10–U38 long-range interaction as a key modulator of the U48 pause in the absence of transcription factor (Fig. 3F), we hypothesized that the same RNA structure could also modulate NusA-mediated stabilization of RNAP pausing. Indeed, the observed effect of F⁻ was abolished when the transcription was performed in the U38A mutant context, whereas the modulation of NusA activity through ligand binding was partially restored with the A10U/U38A compensatory mutant (∼5-fold and only ∼1.5-fold enhancement of U48 pause half-life in the absence and presence of ligand, respectively; Fig. 3G and *SI Appendix*, Table S5). Interestingly, while the U38A mutant no longer allows F⁻ to prevent transcription termination, the A10U mutant and the A10U/U38A compensatory mutant showed a similar ligand sensing activity as WT (Fig. 3E and *SI Appendix*, Fig. S5D and Table S2). In addition, the A10U mutant no longer displayed any significant effect of ligand binding on the relative NusA-mediated pause enhancement (Fig. 3G and *SI Appendix*, Table S5), together suggesting that the A10–U38 long-range interaction modulates both pausing efficiency and NusA activity. Therefore, the effect of NusA on the U48 pause suggests that this particular pause is critical for downstream riboswitch-mediated transcription regulation.

Overall, our data are consistent with a pausing regulation system in which the formation of a ligand-mediated RNA structure modulates transcriptional pausing efficiency and impedes NusA-mediated stabilization of transcriptional pausing.

Riboswitch Folding Modulates NusA Recruitment to PEC. In order to stabilize RNAP pausing, NusA recognizes the RNAP in the paused state and has been suggested to assist with the nucleation of an RNA hairpin inside the RNA exit channel of the enzyme (27). To pinpoint how NusA activity is modulated at the U48 pause, we examined the dynamics of NusA interaction with PEC-48 through a single-molecule colocalization assay (Fig. 4). For this experiment, we purified a NusA protein containing only one single accessible cysteine residue and fluorescently labeled it with Cy5-monomaleimide (NusA-Cy5) (*Methods*). Structural models of NusA bound to the well-characterized *his*-PEC [Protein Data Bank: 6FLQ (27)] suggest that neither the introduced mutations nor the presence of the Cy5 fluorescent dye should impact NusA function (*SI Appendix*, Fig. S6A). Consistent with this expectation, the presence of NusA-Cy5 during the transcription of the F⁻ riboswitch showed the same effect on the T₅₀ value as the unlabeled NusA protein (*SI Appendix*, Fig. S6B and Table S2). To obtain a fluorescently labeled PEC for single-molecule analysis, we initiated transcription with the Cy3-labeled ApU dinucleotide on a DNA template containing a biotin moiety on the 5′-end of the template DNA strand (Fig. 4A). Addition of streptavidin results in the formation of a stable PEC upon addition of all rNTPs that can be immobilized on PEG-passivated quartz slides for imaging via TIRF microscopy (Fig. 4B).

Upon direct excitation of Cy5, we observed short spikes of red fluorescence signal, indicating surprisingly transient binding and dissociation of NusA-Cy5 to PEC-48 (Fig. 4 C and D). We observed fewer detectable binding events in a control experiment in which a 20-fold excess of unlabeled NusA is added concurrently with NusA-Cy5 (*SI Appendix*, Fig. S6 C and D and Table S6). To ask whether the transient nature of NusA binding events to a PEC is universal, we analyzed the dynamic recruitment of NusA to the well-characterized *his*-PEC (27). In that context, similar transient binding events were observed, supporting the highly dynamic NusA binding to PECs in general (*SI Appendix*, Fig. S7). Notably, the *his*-PEC favored more frequent and longer NusA binding events compared to PEC-48, likely due to the structural properties of its hairpin pause signal (*SI Appendix*, Fig. S7A) that previously have been

shown to be critical for NusA-mediated enhancement of RNAP pausing (29).

We calculated the τ_{bound} and $\tau_{unbound}$ dwell times of NusA in the absence and presence of ligand at PEC-48 (Fig. 4E). The resulting cumulative dwell time distributions were fitted with a single-exponential function for k_{on} and to a double-exponential function for k_{off}. In the absence of F⁻, NusA binds with a k_{on} of $7.05 \pm 0.82 \times 10^6$ M⁻¹ s⁻¹, very similar to the overall association rate constant calculated for the *his*-PEC ($7.00 \pm 1.87 \times 10^6$ M⁻¹ s⁻¹; *SI Appendix*, Table S6). In the presence of ligand, a twofold decrease in the k_{on} value was observed ($4.10 \pm 0.11 \times 10^6$ M⁻¹ s⁻¹), indicating that the riboswitch structure in the ligand-bound state prevents NusA recruitment to PEC-48. Interestingly, no significant change in the dissociation rate constant was detected when F⁻ was present (Fig. 4E, *Inset*), demonstrating that ligand binding affects the early steps of NusA-mediated enhancement of pausing by preventing initial NusA recruitment to the PEC. The observed decrease of the k_{on} in the presence of ligand is specific to the riboswitch conformation in the context of PEC-48 since no change in NusA binding kinetics was detected with a PEC paused upstream before the riboswitch is transcribed (EC-25) (*SI Appendix*, Fig. S8 and Table S6). Moreover, NusA recruitment to PEC-72 is promoted in the ligand-free state, probably because of the formation of a more stable terminator hairpin in the RNA exit channel (*SI Appendix*, Fig. S9 and Table S6). These data support the general role of NusA during transcription termination (25).

We further analyzed NusA binding kinetics to PEC-48 in the context of the A10–U38 mutants (Fig. 4F). As expected from our in-bulk time-pausing assays (Fig. 3), the effect of F⁻ on NusA association was strictly dependent on the formation of the A10–U38 long-range interaction in the ligand-bound state. In addition, we noticed a significant (twofold) decrease of k_{on} in the absence of ligand for the U38A mutant relative to WT (Fig. 4F). These results suggest that the introduced mutation alter the properties of the NusA RNA binding site. It was previously suggested that NusA preferentially recognizes stretches of pyrimidine residues in the RNA exit channel (34, 48). Indeed, introduction of the single A10U mutation, which conserves the pyrimidine content of the nascent transcript inside the RNA exit channel, resulted in a significant increase of the NusA association rate constant over WT (Fig. 4F and *SI Appendix*, Table S6). Interestingly, NusA binds to the A10U mutant with two distinct k_{on} values and a significant contribution (>35%) of the fast rate constant to the overall k_{on} (*SI Appendix*, Table S6). This result suggests that the A10–U38 long-range interaction inherently participates in NusA kinetics in the WT construct by preventing the fast association rate component.

Collectively, these data suggest that formation of the A10–U38 long-range interaction is dynamic and that this interaction contributes to the overall association of NusA to PEC-48 in the absence of F⁻. Our single-molecule assays demonstrate how riboswitch cotranscriptional folding modulates the highly dynamic binding of NusA at the U48 pause site and that higher-order RNA structures formed in the vicinity of the RNA exit channel can prevent NusA from being actively recruited to the PEC.

Ligand Binding to the Riboswitch Promotes NusA Release During Transcription Elongation. Our results so far reveal that in the context of a stalled or paused EC, the observed binding kinetics of NusA are readily reversible. This finding suggests that NusA has the potential to modulate EC activity and the transcription rate with a fast response time. We therefore aimed to follow NusA binding during active transcription elongation. To this end, we initiated transcription with a biotinylated dinucleotide (ApU-Biotin) to attach an active halted transcription complex
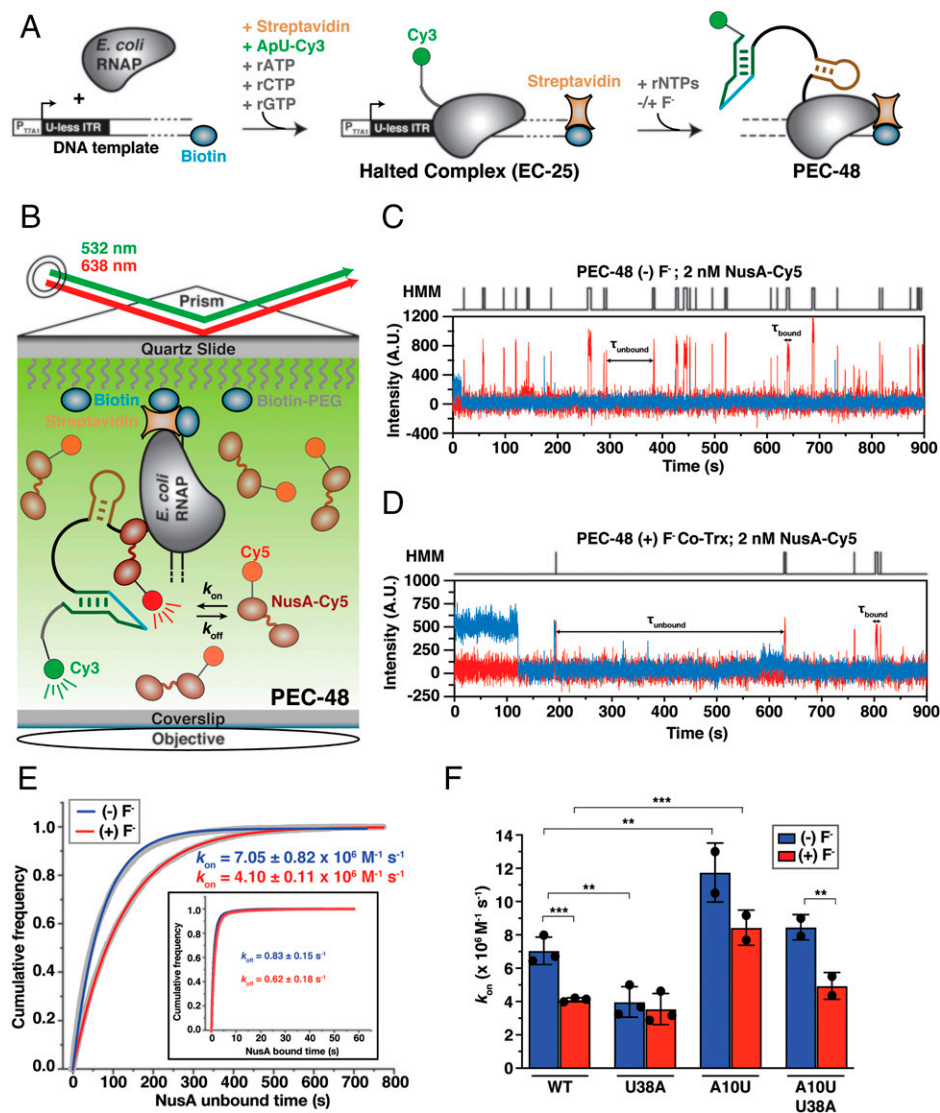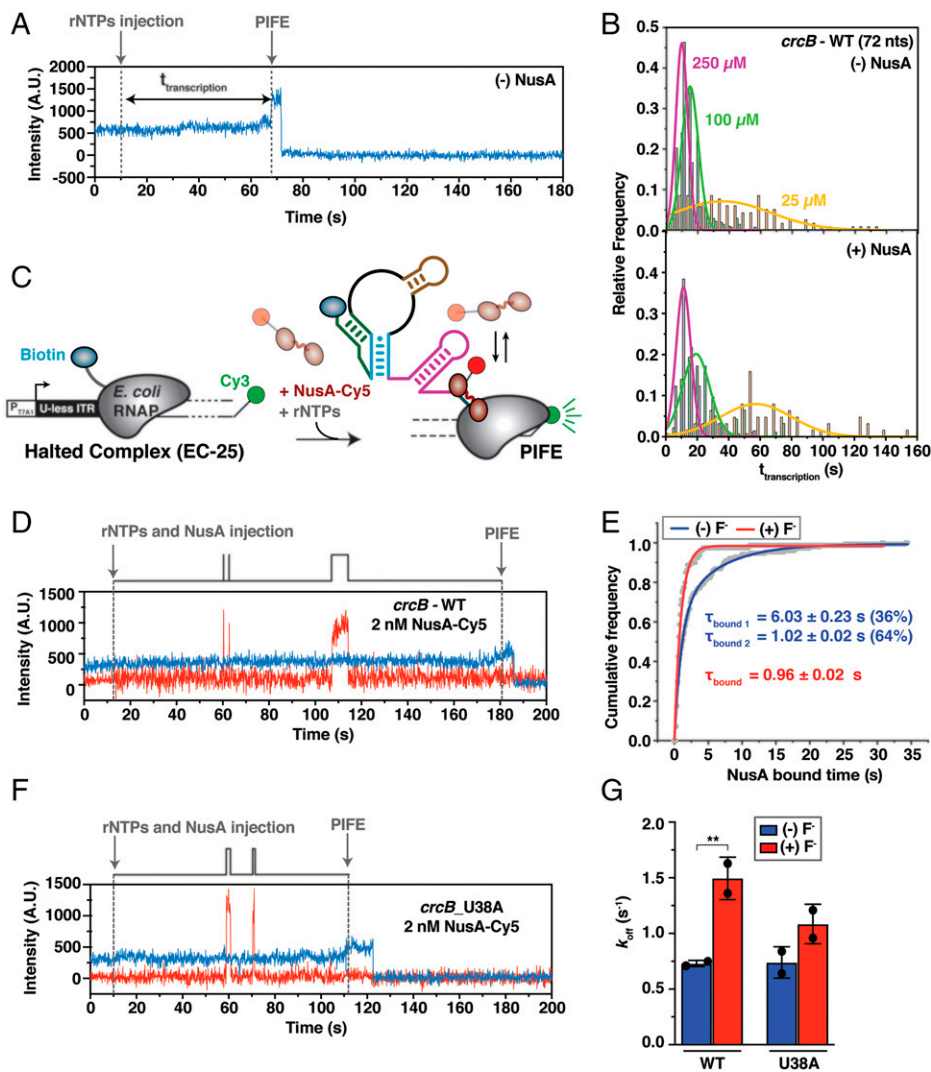
Fig. 4. NusA binds transiently to PECs. (*A*) Fluorescently labeled PECs are transcribed in vitro using *E. coli* RNAP. The halted complex (EC-25) is prepared upon addition of a dinucleotide labeled with Cy3 (ApU-Cy3) and UTP deprivation (ATP/CTP/GTP) to halt the RNAP at the end of the U-less ITR. The biotin-streptavidin interaction at the 3′-end of the DNA template constitutes a stable transcriptional roadblock to stall the RNAP at the desired position. (*B*) Single-molecule setup for studying colocalization of NusA factor labeled with a single Cy5 fluorescent dye (NusA-Cy5) with a PEC. Immobilization of the PEC on the microscope slide occurs through the biotin-streptavidin roadblock. Repeated bindings of NusA-Cy5 to the PEC are monitored upon direct excitation of the Cy5 fluorescent dye. (*C*, *D*) Representative single-molecule trajectories showing the binding of NusA-Cy5 (red) to PEC-48 transcribed in the absence (*C*) or presence (*D*) of 2.5 mM F⁻ ion. HMM is indicated on the top of each trace. (*E*) Plots displaying the cumulative bound (*Inset*) and unbound dwell times of NusA-Cy5 in the absence (blue) and presence (red) of F⁻ ion in the context of PEC-48. The overall binding (k_{on}) and dissociation (k_{off}) rate constants of NusA-Cy5 are indicated. The reported errors are the SD of the mean from independent replicates. Total number of molecules analyzed for each condition is as follows: (−) F⁻ = 532; (+) F⁻ = 675. (*F*) Overall binding rate constants (k_{on}) of NusA-Cy5 in the contexts of the WT, U38A, A10U, and A10U/U38A PEC-48 variants determined in the absence (blue) and presence (red) of 2.5 mM F⁻ ion. Error bars are the SD (SD) of the means from independent replicates. Total number of molecules analyzed for each condition is as follows: WT (−) F⁻ = 532; WT (+) F⁻ = 675; U38A (−) F⁻ = 366; U38A (+) F⁻ = 482; A10U (−) F⁻ = 290; A10U (+) F⁻ = 254; A10U/U38A (−) F⁻ = 250; A10U/U38A (+) F⁻ = 112 (***$P < 0.01$, **$P < 0.05$, *$P < 0.1$).

to a microscope slide via the nascent RNA transcript (49). Similarly to the fluorescently labeled transcript, addition of a biotin moiety to the RNA 5′-end had no significant effect on the ligand-mediated regulation of transcription termination (*SI Appendix*, Fig. S10*A*). In addition, the transcribed DNA was labeled with a Cy3-fluorescent dye at the 5′-end of the template strand, leading to the observation of a protein-induced fluorescence enhancement (PIFE) signal when the RNAP reaches the end of the template (50, 51).

After ~10 s of movie recording, manual injection of the rNTP mix allows for the transcription to restart from the EC-25 stall point, and the PIFE signal was subsequently detected and followed by a loss of the fluorescence signal, indicating transcription to the end of the DNA template, resulting in eventual dissociation of the complex from the surface (Fig. 5*A*). Notably, in some instances we observed that the fluorescence signal returns to its initial intensity (*SI Appendix*, Fig. S10*B*), suggesting that the RNAP may be more strongly blocked by the presence of the fluorescent dye at the very end of the DNA template or that the RNAP potentially could have backtracked or transcribed away from the Cy3-label in the antisense direction (52, 53).

The calculation of the time window between the rNTP injection and the observation of the PIFE signal is equivalent to the amount of time it takes a single RNAP to traverse the DNA template (hereafter referred as $t_{transcription}$). The $t_{transcription}$ values could be well fitted with a single Gaussian distribution consistent with a processive transcription elongation as observed for T7 RNAP (54). As expected (49, 54), decreasing the rNTP concentration led to a significant decrease in the observed overall transcription rate, supporting the notion that we are surveying transcription elongation in real-time (Fig. 5*B* and *SI Appendix*, Fig. S10*D*). We observed a slight increase in the overall transcription rate in the presence of F⁻ compared to the ligand-free condition, potentially due to the absence of strong RNAP pausing at the U72 position in the ligand-bound state (*SI Appendix*, Fig. S10*C*). Addition of a saturating concentration of NusA (0.1 μM) with the transcription mix led to a slight but significant decrease of the transcription rate, which was further enhanced at the lowest rNTP concentration (Fig. 5*B* and *SI Appendix*, Fig. S9*D*). Similar nuanced effects of NusA on the RNAP velocity were previously observed in optical trapping experiments (26), consistent with a model wherein

Chauvier et al.
Dynamic competition between a ligand and transcription factor NusA governs riboswitch-mediated transcription regulation

PNAS | 7 of 12
https://doi.org/10.1073/pnas.2109026118

www.manaraa.com

Fig. 5. Cotranscriptional ligand binding promotes NusA dissociation during transcription. (*A*) Representative single-molecule trajectory showing the real-time transcription of the F⁻ riboswitch. The amount of time between the injection of the rNTPs and the detection of the PIFE signal corresponds to the length of transcription (t_{transcription}). (*B*) Histograms of transcription times obtained using different rNTP concentrations during the transcription of the F⁻ riboswitch performed in the absence (*Top*) and presence (*Bottom*) of 100 nM NusA factor. Number of molecules in each condition are as follows: 250 μM rNTPs, (−) NusA = 73; 100 μM rNTPs, (−) NusA = 104; 25 μM rNTPs, (−) NusA = 115; 250 μM rNTPs, (+) NusA = 138; 100 μM rNTPs, (+) NusA = 93; 25 μM rNTPs, (+) NusA = 113. (*C*) Transcription of the DNA template labeled with Cy3 at the 3′-end using the *E. coli* RNAP allows the formation and the detection of a fluorescent halted complex (EC-25) attached to the microscope slide through the nascent RNA transcript. Transcription is restarted upon addition of all rNTPs, and addition of NusA-Cy5 in the transcription mix allows surveying cotranscriptional NusA binding in real time. When the RNAP reaches the end of the DNA template, the occurrence of the PIFE signal delimits the cotranscriptional window. (*D*) Representative single-molecule trajectory showing the real-time transcription of the F⁻ riboswitch transcribed in the presence of 2 nM NusA-Cy5. Transcription restart is indicated by rNTP injection, and the end of transcription is indicated by PIFE. Repeated cotranscriptional bindings of NusA-Cy5 are monitored upon direct excitation of the Cy5 fluorescent dye. HMM is indicated on the top of the trace. (*E*) Plot displaying the cumulative bound dwell times of NusA-Cy5 in the absence (blue) and presence (red) of 2.5 mM F⁻ ion during the transcription of the WT riboswitch. τ_{bound} dwell times of NusA-Cy5 to the elongating EC are indicated with the contribution of the fast and slow rate constants in parentheses. The reported errors are the SE of the fit. The total number of molecules analyzed in each dataset is as follows: (−) F⁻ = 97; (+) F⁻ = 67. (*F*) Representative single-molecule trajectory showing the real-time transcription of the U38A riboswitch mutant transcribed in the presence of 2 nM NusA-Cy5. Transcription restart is indicated by rNTPs injection, and the end of transcription is indicated by PIFE. Repeated cotranscriptional bindings of NusA-Cy5 are monitored upon direct excitation of the Cy5 fluorescent dye. HMM is indicated on the top of the trace. (*G*) Overall dissociation rate constants (k_{off}) of NusA-Cy5 in the contexts of the WT and U38A variants calculated in the absence (blue) and presence (red) of 2.5 mM F⁻ ion. Error bars are the SD of the means from independent replicates. The total number of molecules analyzed in each dataset is as follows: WT (−) F⁻ = 97; WT (+) F⁻ = 67; U38A (−) F⁻ = 89; U38A (+) F⁻ = 60 (***$P < 0.01$, **$P < 0.05$, *$P < 0.1$).

NusA-mediated regulation of the transcription rate occurs through transient binding of the transcription factor.

In order to probe how cotranscriptional folding of the F⁻ riboswitch modulates NusA dynamics, we performed single-molecule colocalization of NusA-Cy5 in the context of our real-time transcription assay (Fig. 5*C*). Cotranscriptional NusA binding events were detected and analyzed across the time window between the injection of the transcription mix and the observation of the PIFE signal (t_{transcription}), ensuring that the observed binding events were obtained cotranscriptionally (Fig. 5*D*). In the absence of ligand, NusA remained bound to the EC, with two distinct dwell times (τ_{bound1} = 6.03 ± 0.23 s; τ_{bound2} = 1.02 ± 0.02 s), suggesting that the EC adopts different functional conformations targeted by NusA (*SI Appendix*, Table S8). The two notable bound times match closely the values previously calculated at the two different analyzed PECs (PEC-48 and PEC-72), which further supports the model of dynamic NusA binding to ECs engaged in transcription.

When real-time transcription experiments were performed in the presence of F⁻, only the shorter-lived NusA binding events (~1 s) were detected (Fig. 5*E* and *SI Appendix*, Table S8). We hypothesize this observation to reflect cotranscriptional stabilization of the A10–U38 long-range interaction, which then promotes NusA release during active transcription elongation. To test this hypothesis, we analyzed the kinetics of NusA binding during active transcription of the U38A mutant in which ligand sensing activity is abolished (Fig. 5*F*). In the absence of F⁻, NusA still binds cotranscriptionally to the EC with two distinct τ_{bound} values, similar to the WT (*SI Appendix*, Table S8). However, no significant effect of F⁻ was observed on the overall NusA τ_{bound} value (Fig. 5*G* and *SI Appendix*, Table S8), further supporting the model that cotranscriptional ligand binding followed by the formation of the A10–U38 long-range interaction is responsible for NusA release from the transcribing EC.

Taken together, these results unveil multiple complementary mechanisms by which the F⁻ riboswitch fine-tunes the rate of

transcription, in which ligand-induced structural changes of the RNA modulate both the processivity of RNAP through transcriptional pausing modulation and NusA occupancy during transcription elongation.

Discussion

In this work, we have combined biochemical transcription and single-molecule fluorescence microscopy assays to study the dynamic interplay between the general transcription factor NusA and cotranscriptional folding of the F^- riboswitch. Our single-molecule data provide dynamic information that has been absent from a recent burst of structural snapshots highlighting the mechanisms of factor-mediated RNAP pausing (21, 22, 27, 55–58) and how transcription factors are influenced by RNA cotranscriptional folding, revisiting our current model of factor-mediated regulation of transcription. Furthermore, by tracking NusA recruitment during active transcription elongation, we reveal a transcriptional checkpoint at which the F^- riboswitch integrates diverse signals in order to modulate RNAP processivity and ultimately allow for an adaptive genetic response to environmental cues (Fig. 6).

In particular, we reveal that the presence of NusA during the transcription of the F^- riboswitch prevents antitermination induced by ligand binding, pushing the genetic response toward the termination of transcription (Fig. 1). Mechanistically, dynamic sampling of the terminator stem by NusA is shifted toward the adoption of a more stable termination-prone hairpin in the presence of both NusA and F^- (Fig. 2). This observation is consistent with the proposed chaperoning effect of NusA in assisting hairpin folding (27) and a slow transcription regime induced by the presence of NusA (26, 43, 44). Our kinetic insights may help explain how NusA promotes the termination of transcription in vivo, especially at weak, suboptimal terminators (25).

Riboswitch cotranscriptional folding potentially could be facilitated by RNAP pausing, which allows more time for an RNA transcript to adopt a specific and functional conformation (13, 59, 60) or to bind its cognate ligand (11, 36). Transcriptional pausing has been found to be stabilized by two main mechanisms: hairpin-stabilized (class I) and backtracked (class II) (61). In addition, a third class of transcriptional pausing regulation (class III) has been recently identified in the $preQ_1$-sensing riboswitch from *B. subtilis*, in which folding of a pseudoknotted RNA inside the RNA exit channel modulates RNAP pausing efficiency differentially in the absence and presence of ligand (10). Class I pauses are further stabilized by the NusA transcription factor upon interaction with the nascent RNA paused hairpin and the β-flap domain of the RNAP, resulting in the stabilization of the swiveled conformation of the RNAP (27, 62). Class II pauses instead are due to a reverse motion of the RNA relative to the enzyme (backtracking) and lead to the disengagement of the RNA 3′-end from the RNAP catalytic site. This class of pause is sensitive to GreB, which promotes RNA cleavage and subsequent transcription reactivation (63). Class II pauses are also sensitive to NusG, which suppresses backtracking (64). Our results demonstrate that the U48 pause shares similarities with the canonical class I pause, in which folding of the upstream RNA hairpin P3 stabilizes RNAP pausing. Notably, the first base pair of the P3 stem is at the same distance from the RNA 3′ end (65), and a similar enhancement of pausing efficiency is observed in the presence of NusA as for the well-characterized *his*-PEC (66). However, we also found that the U48 pause is further stabilized in the presence of ligand because of the formation of the A10–U38 long-range interaction in the ligand-bound state, analogous to the class III mechanism (Fig. 3). Strikingly, the presence of the same higher-order structure decreases the sensitivity of the
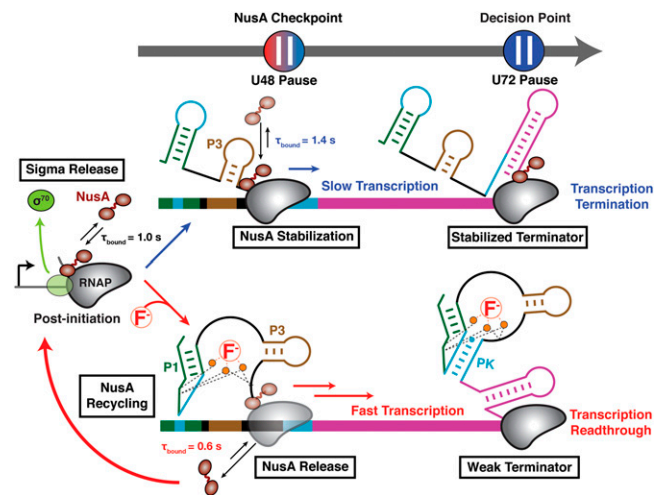
Fig. 6. Model illustrating the dynamic interplay between NusA and the F^- ion during riboswitch-mediated regulation of gene expression. During the elongation of transcription, NusA binds transiently to the EC, fine-tuning the rate of transcription. Transcription can follow two different pathways depending on the presence of a saturating concentration of F^- in the cellular environment. The U48 pause constitutes a transcriptional checkpoint at which NusA is either stabilized or released from the EC. In the absence of F^- (*Upper*), NusA remains bound to the EC for the time frame of transcription so that cotranscriptional folding of the stable terminator hairpin is favored because of slow transcription. Cotranscriptional folding of the riboswitch in the ligand-bound state (*Lower*), by contrast, promotes NusA release from the EC and its recycling and inhibits downstream transcriptional pausing. As a result, the F^- ion acts as a "release factor" that fastens the transcription rate in order to weaken the terminator hairpin and ultimately promote transcription readthrough. Magnesium ions that coordinate ligand binding to the aptamer are indicated as orange spheres based on previous crystal structure of a related riboswitch (47).

PEC to NusA. This observation supports a pivotal role for the U48 pause in the regulation of gene expression. Accordingly, alterations to the long-range A10–U38 interaction in the riboswitch abolish the effect of F^- on RNAP pausing, transcription factor activity, and termination of transcription (Fig. 3).

Few studies have probed NusA activity in the presence of higher-order nascent RNA structures. To our knowledge, previous studies have been restricted to deciphering the mechanism by which NusA interacts with a hairpin-stabilized pause signal or artificial duplexes in the vicinity of the RNA exit channel (65, 67, 68). Interestingly, introduction of the U38A mutation leads to a significantly slower association rate of NusA to PEC-48 in the absence of F^- (Fig. 4F), suggesting that the A10–U38 long-range interaction acts as a key structural switch that masks the NusA binding site on the nascent RNA transcript. The same type of "binding site occlusion" mechanism has been characterized for other riboswitch-mediated regulation systems; for instance, ligand binding to the thiamin pyrophosphate or Mg^{2+}-sensing riboswitches alters the accessibility of the *rut* (Rho-utilization) site for Rho termination factor binding (5, 6), as well as the cleavage sites targeted by RNase E in the lysine and the guanidine-sensing riboswitches (69, 70), supporting the notion that riboswitches can integrate multiple cues to fine-tune their genetic response.

From the broader perspective of the transcription cycle, the surprisingly dynamic sampling of the EC by NusA allows the transcription factor to dynamically modulate the transcription rate. In fact, a fast dissociation of NusA from the EC allows the RNAP to escape from the paused state and thus prevents the accumulation of an irreversibly stalled EC, which otherwise could collide with the DNA replication machinery (71). Moreover, dynamic sampling of the EC by NusA presents an

Chauvier et al.
Dynamic competition between a ligand and transcription factor NusA governs riboswitch-mediated transcription regulation

PNAS | 9 of 12
https://doi.org/10.1073/pnas.2109026118

opportunity for cotranscriptional regulation to occur in a short timeframe. When the RNAP reaches the U48 pause, NusA binds less efficiently if the F$^-$ ion is already bound to the riboswitch (Fig. 4E). While no significant alteration of the RNA structure was detected at the U48 pause site (9), a twofold decrease in the k_{on} was observed in the presence of ligand, supporting the model that NusA is able to distinguish between two slightly shifted conformational equilibria (41).

Conversely, our real-time kinetic analysis of NusA's cotranscriptional binding reveals how F$^-$ prevents NusA-mediated termination of transcription. While two distinct populations of NusA-bound ECs were detected during ligand-free transcription, a significant proportion (>35%) remain tightly associated with NusA (for ∼6 s; Fig. 5E). Assuming a typical average transcription rate of 20 to 25 nt/s in *E. coli* (72) and the high concentration of NusA inside the cell [∼6.5 µM (73)], only ∼3 s would be necessary to complete the transcription of the F$^-$ riboswitch, suggesting that the same molecule of NusA would be present throughout the entire riboswitch synthesis, thus promoting the downstream transcription termination in kinetically aligned fashion (25). Strikingly, NusA dissociates from the EC faster in the presence of F$^-$, with only one population detectable (τ_{bound} ∼1 s), suggesting that ligand binding and RNA structure modulation release NusA cotranscriptionally, allowing efficient recycling of the transcription factor in order to bind and regulate another transcription unit (Fig. 6). Real-time transcription of the U38A mutant supports this hypothesis with an equal distribution of the short and long binding events (Fig. 5F). Our observations thus provide direct evidence for the regulatory contribution of an RNA's cotranscriptional folding and demonstrate how RNA structure modulates the processivity of the transcriptional machinery, which has proven difficult to probe using bulk techniques (16, 20, 56).

In summary, we here have demonstrated a dynamic interplay between ligand and transcription factor binding to a riboswitch, which we anticipate will govern transcription of numerous noncoding RNAs across organisms (74, 75). Using a combination of biochemical and biophysical approaches that are easily transferable to other transcription machineries, we discovered that in the absence of ligand, NusA is able to slow elongation by RNAP and ultimately promote efficient termination of transcription. By contrast, ligand binding to the riboswitch speeds up RNAP transcription via inhibition of transcriptional pausing, mediated in part by rapid cotranscriptional release of NusA factor prior to reaching the termination point (Fig. 6). Our results reveal an unexpected kinetic layer of gene regulation induced by RNA cotranscriptional folding that may be exploited for the design of antibiotic drugs targeting essential factors of the bacterial transcription machinery (40).

Methods

Single-Round In Vitro Transcription Assays. Halted complexes (EC-25) were prepared in transcription buffer (20 mM Tris·HCl, pH 8.0, 20 mM NaCl, 20 mM MgCl$_2$, 14 mM 2-mercaptoethanol, 0.1 mM ethylenediaminetetraacetic acid [EDTA]) containing 25 µM ATP/CTP mix, 50 nM α^{32}P-GTP (3,000 Ci/mmol), 10 µM ApU dinucleotide primer (Trilink), and 50 nM DNA template. *E. coli* RNAP holoenzyme (New England Biolabs) was added to 100 nM, and the mixture was incubated for 10 min at 37 °C. The sample was passed through a G50 column to remove any free nucleotides. To complete the transcription reaction, all four rNTPs were added concomitantly with heparin (450 µg/mL) to prevent the reinitiation of transcription. Time-pausing experiments were performed using 10 µM rNTPs. For termination assays, the F$^-$ concentrations ranged from 1 µM to 10 mM. The mixture was incubated at 37 °C, and reaction aliquots were quenched at the desired times into an equal volume of loading buffer (95% formamide, 1 mM EDTA, 0.1% sodium dodecyl sulfate [SDS], 0.2% bromophenol blue, 0.2% xylene cyanol). Sequencing ladders were prepared by combining the halted complex with a chase solution containing 250 µM of each rNTP, in addition to one 3′-OMe rNTP (at 5 µM for 3′-OMe GTP and 2 µM for 3′-OMe ATP, UTP, and CTP).

Reaction aliquots were denatured before loading 5 to 8 µL of each onto a denaturing 8 M urea, 6% polyacrylamide sequencing gel. The gel was dried and exposed to a phosphor screen (typically overnight), which was then scanned on a Typhoon Phosphor Imager (GE Healthcare).

Transcription Data Analysis. To determine the T$_{50}$, the relative intensity of the full-length product was divided by the total amount of RNA transcript (full-length + terminated product) for each F$^-$ concentration. The resulted percentages of readthrough were plotted against the ligand concentration using equation

$$Y = Y_0 + ((M1 * X)/(T_{50} + X)),$$

where Y$_0$ is the value of Y at X$_{min}$ (no ligand condition) and M1 = Y$_{max}$ − Y$_{min}$

The half-life of transcriptional pausing was determined by calculating the fraction of each RNA pause species compared with the total amount of RNA for each time point, which was analyzed with pseudo-first–order kinetics to extract the half-life (76). For each determination, we have subtracted the background signal.

Preparation of Fluorescently Labeled Nascent Transcripts. In vitro transcription reactions were performed in two steps to allow the specific incorporation of Cy3 at the 5′-end of the RNA sequence. Transcription reactions were performed in the same transcription buffer described above. Transcription reactions were initiated by adding 100 µM ApU-Cy3 dinucleotide and 25 µM ATP/CTP/GTP nucleotides at 37 °C for 10 min, thus yielding a fluorescent halted complex. The sample was next passed through a G50 column to remove any free nucleotides, and the transcription was resumed upon addition of all four rNTPs at the indicated concentration and heparin (450 µg/mL) to prevent the reinitiation of transcription. The resulted nascent transcript was hybridized to the 5′-biotinylated CP (Anchor_Bio oligonucleotide) complementary to the 3′-end capture sequence, allowing immobilization of the complex to the microscope slide. The CP was mixed to a ratio of 10:1 with RNA transcript and added for 5 min before flowing the whole complex to the microscope slide.

In the case of PEC transcription, the DNA templates contain a biotin at the 5′-end of the template DNA strand. Streptavidin was mixed to a ratio of 5:1 with the DNA template for 5 min prior to start the transcription reaction.

F$^-$ (when present) was always added cotranscriptionally (except for the posttranscriptional experiment in Fig. 2E) at a final concentration of 2.5 mM, and the same concentration of ligand was added into the corresponding buffer during subsequent dilutions.

NusA Expression and Purification. WT and single-cysteine NusA were expressed from plasmids pNG5 and pKH3, respectively, in BLR (DE3) cells. The cells were grown in Luria Bertani media supplemented with 50 µg/mL kanamycin, induced with 1 mM isopropyl Beta-d-1-thiogalactopyranoside when optical density at 600 nm reached ∼0.7 and harvested 3 h postinduction. His-tagged proteins were purified using nickel affinity chromatography as described previously (28). The fractions containing NusA protein were confirmed by SDS polyacrylamide gel electrophoresis (PAGE) and dialyzed into low salt dialysis buffer (20 mM Tris·HCl, pH 8.0, 200 mM NaCl, 0.5 mM Tris(2-carboxyethyl)-phosphine hydrochloride [TCEP], 0.1 mM Na$_2$EDTA) and subsequently purified using ion-exchange chromatography (Mono Q) using an NaCl gradient from 0.2 M to 2 M. In the case of the single-cysteine mutant, the ion-exchange chromatography was performed after the labeling step (see *NusA Labeling*). After purification, the protein was found to be purified to >95% homogeneity and mixed in a 1:1 ratio with storage buffer (20 mM Tris·HCl, pH 8.0, 200 mM NaCl, 0.5 mM TCEP, 0.1 mM Na$_2$EDTA, 50% glycerol) and flash frozen in liquid nitrogen for storage at −80 °C.

NusA Labeling. NusA was labeled with Cy5-maleimide dye (PA25031, GE Healthcare) using an 8:1 molar ratio of dye/protein in a total volume of 200 µL (∼20 µM protein) of labeling buffer (20 mM Tris·HCl, pH 8.0, 200 mM NaCl, 0.5 mM TCEP, 0.1 mM Na$_2$EDTA). After ∼4.5 h incubation at 4 °C, the reaction was quenched upon addition of excess 2-mercaptoethanol. NusA-Cy5 and the free dye were separated by ion-exchange chromatography. The labeling reaction was loaded on a Mono Q column and washed with excess amount (over 20 column volume) of ion-exchange buffer (20 mM Tris·HCl, pH 8.0, 200 mM NaCl, 0.5 mM TCEP, 0.1 mM Na$_2$EDTA) to remove the free dye. Then, NusA-Cy5 was eluted from the column using an NaCl gradient from 0.2 M to 2 M. The fractions containing NusA protein were confirmed by SDS-PAGE, and the purified labeled protein was mixed in 1:1 ratio with storage buffer (20 mM Tris·HCl, pH 8.0, 200 mM NaCl, 0.5 mM TCEP, 0.1 mM Na$_2$EDTA, 50% glycerol) and flash frozen for storage at −80 °C. Labeling stoichiometry was determined as ∼0.6 for Cy5/NusA using the absorbance measurements at A$_{280}$ and A$_{650}$.

www.manaraa.com

Single-Molecule Experiments. All single-molecule fluorescence microscopy experiments were performed using a prism-based TIRF microscope based on an Olympus IX-71 frame equipped with a 60× water-immersion objective (Olympus UPlanApo, 1.2 NA). All movies were collected at 100-ms time resolution using an intensified charge-coupled device camera (Hamamatsu C13440-20CU scientific complementary metal-oxide semiconductor camera). PEG-passivated quartz slides with a microfluidic channel containing inlet and outlet ports for buffer exchange were assembled as described in previous works (45, 77). For real-time transcription assay, the inlet consists of a cut pipet tip acting as a reservoir, and the outlet is connected to a 3-mL syringe to pull in the solution to the microscope slide. The surface of the microfluidic channel was coated with streptavidin (0.2 mg/mL) for 10 to 15 min prior to flowing the nascent transcripts hybridized to the CP or the halted complex for real-time transcription. In the case of PEC analysis, the fluorescent PECs were directly injected into the channel surface using the biotin-streptavidin roadblock for immobilization.

For SiM-KARTS experiments, the nascent RNA transcripts were diluted in SiM-KARTS buffer (80 mM Hepes-KOH, pH 7.5, 300 mM KCl, 5 mM MgCl$_2$).

For NusA colocalization assays and real-time transcription, the molecules were diluted in imaging buffer (40 mM Tris·HCl, pH 8.0, 330 mM KCl, 5 mM MgCl$_2$, 0.1 mM EDTA, 0.1 mM dithiothreitol, 1 mg/mL bovine serum albumin).

NusA-Cy5 (2 nM) or the SiM-KARTS probe (12.5 nM) was injected into the channel in the corresponding imaging buffer along with an enzymatic oxygen scavenging system consisting of 44 mM glucose, 165 U/mL glucose oxidase from *Aspergillus niger*, 2,170 U/mL catalase from *Corynebacterium glutamicum*, and 5 mM Trolox to extend the lifetime of the fluorophores and to prevent photo-blinking of the dyes (10). For real-time transcription assays, the oxygen scavenging system was injected prior to the addition of the transcription mixture to stabilize the lifetime of the molecules at the beginning of the recording. To perform in-slide transcription, heparin (450 μg/mL), rNTPs, and NusA (2 nM for NusA-Cy5 or 100 nM for unlabeled NusA) were carefully injected after ~10 s recording.

The raw movies were collected for 10 to 15 min with direct green (532 nm) and red (638 nm) laser excitation.

Single-Molecule Data Analysis. Locations of molecules and fluorescence intensity traces for each molecule were extracted from raw movie files using custom-built MATLAB codes (MathWorks). Traces were manually selected in MATLAB for further analysis using the following criteria: single-step photobleaching of Cy3 and ≥2 spikes of Cy5 fluorescence of more than twofold the background intensity. Traces showing binding events were idealized using a two-state (bound and unbound) model using a segmental *k*-means algorithm in QuB (78, 79). From the idealized traces, dwell times of NusA or the SiM-KARTS probe in the bound (τ_{bound}) and the unbound ($\tau_{unbound}$) states were

obtained. Cumulative of bound and unbound dwell time distributions were plotted and fitted in OriginLab with single-exponential or double-exponential functions to obtain the lifetimes in the bound and unbound states. The dissociation rate constants (k_{off}) were calculated as the inverse of the τ_{bound}, whereas the binding rate constants (k_{on}) were calculated by dividing the inverse of the $\tau_{unbound}$ by the concentration of NusA-Cy5 or SiM-KARTS probe used during the data collection. Statistical significance of differences in the rate constants was determined using two-tailed Student's test (*t* test). *P* values < 0.1 were considered significant.

Determining the Transcription Rate. To assess the end of the transcription process, each Cy3 trajectory was inspected manually to observe the PIFE signal. A PIFE signature marking the end of transcription is defined as a sharp increase in the fluorescence intensity. In most cases, the PIFE signal is followed shortly after by a loss of Cy3 intensity, indicating either dissociation of the labeled DNA from the EC or photobleaching of the Cy3 fluorescent dye. The transcription time or the time interval between the rNTP injection and the observation of the PIFE signature could be well fitted using a single Gaussian function in OriginLab. Traces exhibiting multiple PIFE peaks were not analyzed because these molecules likely represent more than one single EC or the presence of two RNAPs on the same DNA template. The exact time point marking the end of transcription was selected as the time frame when the higher Cy3 intensity was detected (54). The transcription rate was calculated by dividing the length of the transcribed RNA (72 nucleotides) by the transcription time.

For cotranscriptional NusA binding assays, traces were first filtered for a PIFE signal, then molecules showing at least one NusA-Cy5 binding event were collected for further kinetics analysis as described above.

Statistical Details. Statistical details of individual experiments such as number of molecules analyzed and definition of error bars are indicated in the main text, figures, and figure legends.

1. E. Bakkeren, M. Diard, W.-D. Hardt, Evolutionary causes and consequences of bacterial antibiotic persistence. *Nat. Rev. Microbiol.* **18**, 479–490 (2020).
2. A. V. Sherwood, T. M. Henkin, Riboswitch-mediated gene regulation: Novel RNA architectures dictate gene expression responses. *Annu. Rev. Microbiol.* **70**, 361–374 (2016).
3. A. V. Bédard, E. D. M. Hien, D. A. Lafontaine, Riboswitch regulation mechanisms: RNA, metabolites and regulatory proteins. *Biochim. Biophys. Acta. Gene Regul. Mech.* **1863**, 194501 (2020).
4. A. Ray-Soni, M. J. Bellecourt, R. Landick, Mechanisms of bacterial transcription termination: All good things must end. *Annu. Rev. Biochem.* **85**, 319–347 (2016).
5. A. Chauvier et al., Transcriptional pausing at the translation start site operates as a critical checkpoint for riboswitch regulation. *Nat. Commun.* **8**, 13892 (2017).
6. K. Hollands et al., Riboswitch control of Rho-dependent transcription termination. *Proc. Natl. Acad. Sci. U.S.A.* **109**, 5376–5381 (2012).
7. K. Hollands, A. Sevostiyanova, E. A. Groisman, Unusually long-lived pause required for regulation of a Rho-dependent transcription terminator. *Proc. Natl. Acad. Sci. U.S.A.* **111**, E1999–E2007 (2014).
8. J. L. Baker et al., Widespread genetic switches and toxicity resistance proteins for fluoride. *Science* **335**, 233–235 (2012).
9. K. E. Watters, E. J. Strobel, A. M. Yu, J. T. Lis, J. B. Lucks, Cotranscriptional folding of a riboswitch at nucleotide resolution. *Nat. Struct. Mol. Biol.* **23**, 1124–1131 (2016).
10. J. R. Widom et al., Ligand modulates cross-coupling between riboswitch folding and transcriptional pausing. *Mol. Cell* **72**, 541–552.e6 (2018).
11. J. K. Wickiser, W. C. Winkler, R. R. Breaker, D. M. Crothers, The speed of RNA transcription and metabolite binding kinetics operate an FMN riboswitch. *Mol. Cell* **18**, 49–60 (2005).
12. C. Helmling et al., Life times of metastable states guide regulatory signaling in transcriptional riboswitches. *Nat. Commun.* **9**, 944 (2018).
13. G. A. Perdrizet II, I. Artsimovitch, R. Furman, T. R. Sosnick, T. Pan, Transcriptional pausing coordinates folding of the aptamer domain and the expression platform of a riboswitch. *Proc. Natl. Acad. Sci. U.S.A.* **109**, 3323–3328 (2012).
14. S. Chatterjee, A. Chauvier, S. S. Dandpat, I. Artsimovitch, N. G. Walter, A translational riboswitch coordinates nascent transcription-translation coupling. *Proc. Natl. Acad. Sci. U.S.A.* **118**, e2023426118 (2021).
15. S. Proshkin, A. R. Rahmouni, A. Mironov, E. Nudler, Cooperation between translating ribosomes and RNA polymerase in transcription elongation. *Science* **328**, 504–508 (2010).
16. T. Pan, T. Sosnick, RNA folding during transcription. *Annu. Rev. Biophys. Biomol. Struct.* **35**, 161–175 (2006).
17. I. Gusarov, E. Nudler, The mechanism of intrinsic transcription termination. *Mol. Cell* **3**, 495–504 (1999).
18. I. Artsimovitch, R. Landick, The transcriptional regulator RfaH stimulates RNA chain synthesis after recruitment to elongation complexes by the exposed nontemplate DNA strand. *Cell* **109**, 193–203 (2002).
19. M. H. Larson et al., A pause sequence enriched at translation start sites drives transcription dynamics in vivo. *Science* **344**, 1042–1047 (2014).
20. J. Zhang, R. Landick, A two-way street: Regulatory interplay between RNA polymerase and nascent RNA structure. *Trends Biochem. Sci.* **41**, 293–310 (2016).
21. F. Krupp et al., Structural basis for the action of an all-purpose transcription antitermination factor. *Mol. Cell* **74**, 143–157.e5 (2019).
22. Y.-H. Huang et al., Structure-based mechanisms of a molecular RNA polymerase/chaperone machine required for ribosome biosynthesis. *Mol. Cell* **79**, 1024–1036.e5 (2020).
23. U. Vogel, K. F. Jensen, NusA is required for ribosomal antitermination and for modulation of the transcription elongation rate of both antiterminated RNA and mRNA. *J. Biol. Chem.* **272**, 12265–12271 (1997).
24. I. Gusarov, E. Nudler, Control of intrinsic transcription termination by N and NusA: The basic mechanisms. *Cell* **107**, 437–449 (2001).
25. S. Mondal, A. V. Yakhnin, A. Sebastian, I. Albert, P. Babitzke, NusA-dependent transcription termination prevents misregulation of global gene expression. *Nat. Microbiol.* **1**, 15007 (2016).
26. J. Zhou, K. S. Ha, A. La Porta, R. Landick, S. M. Block, Applied force provides insight into transcriptional pausing and its modulation by transcription factor NusA. *Mol. Cell* **44**, 635–646 (2011).

Chauvier et al.
Dynamic competition between a ligand and transcription factor NusA governs riboswitch-mediated transcription regulation

www.manaraa.com

27. X. Guo *et al.*, Structural basis for NusA stabilized transcriptional pausing. *Mol. Cell* **69**, 816–827.e4 (2018).

28. K. S. Ha, I. Toulokhonov, D. G. Vassylyev, R. Landick, The NusA N-terminal domain is necessary and sufficient for enhancement of transcriptional pausing via interaction with the RNA exit channel of RNA polymerase. *J. Mol. Biol.* **401**, 708–725 (2010).

29. I. Toulokhonov, R. Landick, The flap domain is required for pause RNA hairpin inhibition of catalysis by RNA polymerase and can modulate intrinsic termination. *Mol. Cell* **12**, 1125–1136 (2003).

30. T. Pan, I. Artsimovitch, X. W. Fang, R. Landick, T. R. Sosnick, Folding of a large ribozyme during transcription and the effect of the elongation factor NusA. *Proc. Natl. Acad. Sci. U.S.A.* **96**, 9545–9550 (1999).

31. J. Greenblatt, J. Li, Interaction of the sigma factor and the nusA gene protein of *E. coli* with RNA polymerase in the initiation-termination cycle of transcription. *Cell* **24**, 421–428 (1981).

32. T. F. Mah, K. Kuznedelov, A. Mushegian, K. Severinov, J. Greenblatt, The alpha subunit of *E. coli* RNA polymerase activates RNA binding by NusA. *Genes Dev.* **14**, 2664–2675 (2000).

33. R. A. Mooney *et al.*, Regulator trafficking on bacterial transcription units in vivo. *Mol. Cell* **33**, 97–108 (2009).

34. S. Prasch *et al.*, RNA-binding specificity of *E. coli* NusA. *Nucleic Acids Res.* **37**, 4736–4742 (2009).

35. C. Ma *et al.*, RNA polymerase-induced remodelling of NusA produces a pause enhancement complex. *Nucleic Acids Res.* **43**, 2829–2840 (2015).

36. A. Chauvier, J.-F. Nadon, J. P. Grondin, A.-M. Lamontagne, D. A. Lafontaine, Role of a hairpin-stabilized pause in the *Escherichia coli thiC* riboswitch function. *RNA Biol.* **16**, 1066–1073 (2019).

37. J.-F. Lemay *et al.*, Comparative study between transcriptionally- and translationally-acting adenine riboswitches reveals key differences in riboswitch regulatory mechanisms. *PLoS Genet.* **7**, e1001278 (2011).

38. S. Y. Gerdes *et al.*, Experimental determination and system level analysis of essential genes in *Escherichia coli* MG1655. *J. Bacteriol.* **185**, 5673–5684 (2003).

39. K. Kobayashi *et al.*, Essential *Bacillus subtilis* genes. *Proc. Natl. Acad. Sci. U.S.A.* **100**, 4678–4683 (2003).

40. C. Ma, X. Yang, P. J. Lewis, Bacterial transcription as a target for antibacterial drug development. *Microbiol. Mol. Biol. Rev.* **80**, 139–160 (2016).

41. B. Zhao, S. L. Guffy, B. Williams, Q. Zhang, An excited state underlies gene regulation of a transcriptional riboswitch. *Nat. Chem. Biol.* **13**, 968–974 (2017).

42. I. Artsimovitch, V. Svetlov, L. Anthony, R. R. Burgess, R. Landick, RNA polymerases from *Bacillus subtilis* and *Escherichia coli* differ in recognition of regulatory signals in vitro. *J. Bacteriol.* **182**, 6027–6035 (2000).

43. P. H. von Hippel, T. D. Yager, Transcript elongation and termination are competitive kinetic processes. *Proc. Natl. Acad. Sci. U.S.A.* **88**, 2307–2311 (1991).

44. J. C. McDowell, J. W. Roberts, D. J. Jin, C. Gross, Determination of intrinsic transcription termination efficiency by RNA polymerase elongation rate. *Science* **266**, 822–825 (1994).

45. A. Chauvier, J. Cabello-Villegas, N. G. Walter, Probing RNA structure and interaction dynamics at the single molecule level. *Methods* **162–163**, 3–11 (2019).

46. A. J. Rinaldi, P. E. Lund, M. R. Blanco, N. G. Walter, The Shine-Dalgarno sequence of riboswitch-regulated single mRNAs shows ligand-dependent accessibility bursts. *Nat. Commun.* **7**, 8976 (2016).

47. A. Ren, K. R. Rajashankar, D. J. Patel, Fluoride ion encapsulation by Mg^{2+} ions and phosphates in a fluoride riboswitch. *Nature* **486**, 85–89 (2012).

48. M. Z. Qayyum, D. Dey, R. Sen, Transcription elongation factor NusA is a general antagonist of Rho-dependent termination in *Escherichia coli*. *J. Biol. Chem.* **291**, 8090–8108 (2016).

49. O. Duss *et al.*, Real-time assembly of ribonucleoprotein complexes on nascent RNA transcripts. *Nat. Commun.* **9**, 5087 (2018).

50. H. Hwang, S. Myong, Protein induced fluorescence enhancement (PIFE) for probing protein-nucleic acid interactions. *Chem. Soc. Rev.* **43**, 1221–1229 (2014).

51. H. Hwang, H. Kim, S. Myong, Protein induced fluorescence enhancement as a single molecule assay with short distance sensitivity. *Proc. Natl. Acad. Sci. U.S.A.* **108**, 7414–7418 (2011).

52. T. T. Harden *et al.*, Alternative transcription cycle for bacterial RNA polymerase. *Nat. Commun.* **11**, 448 (2020).

53. W. Kang *et al.*, Transcription reinitiation by recycling RNA polymerase that diffuses on DNA after releasing terminated RNA. *Nat. Commun.* **11**, 450 (2020).

54. M. L. Rodgers, S. A. Woodson, Transcription increases the cooperativity of ribonucleoprotein assembly. *Cell* **179**, 1370–1381.e12 (2019).

55. J. Y. Kang *et al.*, Structural basis for transcript elongation control by NusG family universal regulators. *Cell* **173**, 1650–1662.e14 (2018).

56. R. A. Mooney, R. Landick, Tethering sigma70 to RNA polymerase reveals high in vivo activity of sigma factors and sigma70-dependent pausing at promoter-distal locations. *Genes Dev.* **17**, 2839–2851 (2003).

57. N. Said *et al.*, Steps toward translocation-independent RNA polymerase inactivation by terminator ATPase ρ. *Science* **371**, eabd1673 (2021).

58. C. Wang *et al.*, Structural basis of transcription-translation coupling. *Science* **369**, 1359–1365 (2020).

59. C. Helmling *et al.*, NMR structural profiling of transcriptional intermediates reveals riboswitch regulation by metastable RNA conformations. *J. Am. Chem. Soc.* **139**, 2647–2656 (2017).

60. G. Nechooshtan, M. Elgrably-Weiss, S. Altuvia, Changes in transcriptional pausing modify the folding dynamics of the pH-responsive RNA element. *Nucleic Acids Res.* **42**, 622–630 (2014).

61. I. Artsimovitch, R. Landick, Pausing by bacterial RNA polymerase is mediated by mechanistically distinct classes of signals. *Proc. Natl. Acad. Sci. U.S.A.* **97**, 7090–7095 (2000).

62. J. Y. Kang *et al.*, RNA polymerase accommodates a pause RNA hairpin by global conformational rearrangements that prolong pausing. *Mol. Cell* **69**, 802–815.e5 (2018).

63. M. Abdelkareem *et al.*, Structural basis of transcription: RNA polymerase backtracking and its reactivation. *Mol. Cell* **75**, 298–309.e4 (2019).

64. K. M. Herbert *et al.*, *E. coli* NusG inhibits backtracking and accelerates pause-free transcription by promoting forward translocation of RNA polymerase. *J. Mol. Biol.* **399**, 17–30 (2010).

65. I. Toulokhonov, I. Artsimovitch, R. Landick, Allosteric control of RNA polymerase by a site that contacts nascent RNA hairpins. *Science* **292**, 730–733 (2001).

66. S. Kyzer, K. S. Ha, R. Landick, M. Palangat, Direct versus limited-step reconstitution reveals key features of an RNA hairpin-stabilized paused transcription complex. *J. Biol. Chem.* **282**, 19020–19028 (2007).

67. P. P. Hein *et al.*, RNA polymerase pausing and nascent-RNA structure formation are linked through clamp-domain movement. *Nat. Struct. Mol. Biol.* **21**, 794–802 (2014).

68. K. E. Kolb, P. P. Hein, R. Landick, Antisense oligonucleotide-stimulated transcriptional pausing reveals RNA exit channel specificity of RNA polymerase and mechanistic contributions of NusA and RfaH. *J. Biol. Chem.* **289**, 1151–1163 (2014).

69. M.-P. Caron *et al.*, Dual-acting riboswitch control of translation initiation and mRNA decay. *Proc. Natl. Acad. Sci. U.S.A.* **109**, E3444–E3453 (2012).

70. J. Richards, J. G. Belasco, Widespread protection of RNA cleavage sites by a riboswitch aptamer that folds as a compact obstacle to scanning by RNase E. *Mol. Cell* **81**, 127–138.e4 (2021).

71. M. Hawkins *et al.*, Direct removal of RNA polymerase barriers to replication by accessory replicative helicases. *Nucleic Acids Res.* **47**, 5100–5113 (2019).

72. U. Vogel, K. F. Jensen, The RNA chain elongation rate in *Escherichia coli* depends on the growth rate. *J. Bacteriol.* **176**, 2807–2813 (1994).

73. A. Schmidt *et al.*, The quantitative and condition-dependent *Escherichia coli* proteome. *Nat. Biotechnol.* **34**, 104–110 (2016).

74. G. A. Rosen *et al.*, Dynamics of RNA polymerase II and elongation factor Spt4/5 recruitment during activator-dependent transcription. *Proc. Natl. Acad. Sci. U.S.A.* **117**, 32348–32357 (2020).

75. N. Sanchez de Groot *et al.*, RNA structure drives interaction with proteins. *Nat. Commun.* **10**, 3246 (2019).

76. R. Landick, D. Wang, C. L. Chan, Quantitative analysis of transcriptional pausing by *Escherichia coli* RNA polymerase: His leader pause site as paradigm. *Methods Enzymol.* **274**, 334–353 (1996).

77. K. C. Suddala, N. G. Walter, Riboswitch structure and dynamics by smFRET microscopy. *Methods Enzymol.* **549**, 343–373 (2014).

78. M. Blanco, N. G. Walter, Analysis of complex single-molecule FRET time trajectories. *Methods Enzymol.* **472**, 153–178 (2010).

79. F. Qin, L. Li, Model-based fitting of single-channel dwell-time distributions. *Biophys. J.* **87**, 1657–1671 (2004).

Chauvier *et al.*
Dynamic competition between a ligand and transcription factor NusA governs riboswitch-mediat...